Journal of ELECTRONIC MATERIALS, Vol. 44, No. 8, 2015
DOI: 10.1007/s11664-015-3783-8
© 2015 The Minerals, Metals & Materials Society

CrossMark

# Highly Conducting Gallium-Doped ZnO Thin Film as Transparent Schottky Contact for Organic-Semiconductor-Based Schottky Diodes

BUDHI SINGH[1] and SUBHASIS GHOSH[1,2,3]

1.—Electronic Materials and Device Laboratory, School of Physical Sciences, Jawaharlal Nehru University, New Delhi 110067, India. 2.—e-mail: subhasis.ghosh.jnu@gmail.com. 3.—e-mail: subhasis@mail.jnu.ac.in

Highly conducting and transparent Ga-doped ZnO (GZO) thin films have been grown on transparent substrates at different growth temperatures with Ga content varying from 0.01% to 10%. All films showed pronounced $c$-axis orientation corresponding to hexagonal wurtzite structure. The minimum resistivity of $4.3 \times 10^{-4}\ \Omega$ cm was reproducibly obtained in GZO thin film doped with 2% Ga and grown at 600°C. We have further shown that highly conducting transparent GZO thin film can be used as a Schottky contact in copper phthalocyanine (CuPc)-based Schottky diodes. The capacitance–voltage characteristics of the Al/CuPc/Au and GZO/CuPc/Au Schottky diodes show similar built-in potential ($V_{bi}$) of 0.98 V, which is close to the difference in work function between Au (5.2 eV) and Al or GZO (4.2 eV), establishing that GZO behaves as a metal electrode with work function similar to Al. Similar values of acceptor concentration ($\sim 10^{15}$ cm$^{-3}$) in CuPc were obtained from the capacitance–voltage characteristics of the Al/CuPc/Au and GZO/CuPc/Au Schottky diodes. These observations indicate the absence of interface states at the metal/organic interface in CuPc-based Schottky diodes.

**Key words:** ZnO, transparent conducting electrode, organic Schottky diode, built-in potential barrier

## INTRODUCTION

Optical transparency in the visible region and metal-like conductivity are the most useful properties of materials for the development of two different areas of electronics: organic electronics and transparent electronics. Organic electronics includes devices based on polymers and organic molecular semiconductors, such as organic light-emitting diodes (OLEDs), organic field-effect transistors (OFETs), and organic solar cells (OSCs), whereas transparent electronics includes fully transparent devices such as transparent thin-film transistors (TFTs) as well as ZnO-based semitransparent solar cells.[1–6] ZnO is a semiconductor with a direct wide bandgap ($\sim$3.37 eV), a relatively large exciton binding energy of 60 meV, and attractive electrical and optical properties. As-grown undoped ZnO shows $n$-type semiconducting properties due to O vacancies and Zn interstitials.[7] It is impossible to obtain stable $p$-type ZnO, so ZnO-based $p$–$n$ homojunctions are difficult to achieve, whereas $p$-type organic semiconductors are abundant. Therefore, by combining the versatile properties of such organic and inorganic semiconducting materials, one can enhance the functionality of devices beyond that achievable with a single semiconducting material.[8–11] Organic/inorganic hybrid devices based on ZnO and organic semiconductors have attracted strong technological interest for use as hybrid LEDs, solar cells, and FETs by combining the functionality of the wide range of organic materials with the well-established properties of $n$-type ZnO. On the other hand, it is well known that metal–semiconductor junctions play a significant role in the performance of electronic devices

(Received August 8, 2014; accepted April 3, 2015; published online April 22, 2015)

such as FETs, OSCs, and OLEDs. Advancement in transparent technology requires transparent conducting electrodes, for which conducting ZnO is a potential candidate. Also, conducting ZnO is a promising alternative to indium tin oxide (ITO) as a transparent conducting electrode for use in OSCs, OLEDs, TFTs, hybrid diodes, and many other optoelectronics applications due to its low cost and nontoxic nature.[12–16] The conductivity of ZnO can be varied by controlled doping with group III elements (B, Al, Ga, In).[17–21]

In this work, we present how to achieve highly conducting Ga-doped ZnO (GZO) transparent thin films and their application in organic semiconductor-based Schottky diodes. GZO thin films have the following advantages in comparison with Al-doped ZnO (AZO) or In-doped ZnO (IZO) thin films: (i) the Ga–O covalent bond length is nearly the same as that of Zn–O, which leads to less strain in the doped film; (ii) Ga is less reactive than Al and more resistive to oxidation; and (iii) it has been shown that Ga does not exhibit a tendency to segregate at surfaces, interfaces, and extended defects, compared with Al and In, which is crucial for applications requiring superior control over the impurity distribution.[22,23] Highly conducting GZO thin films have been used as transparent conducting electrodes in OLEDs and OSCs.[15,24] In this work, highly conducting, *c*-axis-oriented GZO thin films were achieved by controlling the doping concentration of Ga. Furthermore, highly conducting transparent GZO thin films were successfully employed as Schottky contacts in organic-molecular-based Schottky diodes.

## EXPERIMENTAL PROCEDURES

### Thin-Film Deposition

All GZO thin films were deposited by radiofrequency (RF) magnetron sputtering on transparent quartz substrate. RF magnetron sputtering was chosen over pulsed laser deposition (PLD) for growth of the doped and undoped ZnO thin films due to several advantages such as (i) relatively easy control over doping, (ii) lower cost, and (iii) no limitation on sample area as in the case of PLD.[18] A series of ZnO sputtering targets with different Ga contents from 0.01% to 10% were prepared by the solid-state route. ZnO and $Ga_2O_3$ powder with purity of 99.999%, procured from Sigma Aldrich, were mixed in stoichiometric ratio, ground for 24 h, and sintered at 850°C for 24 h to prepare the sputtering targets. During deposition of the GZO thin films, the target-to-substrate distance was kept at 7 cm. The sputtering chamber was initially evacuated to $10^{-6}$ mbar using a turbomolecular pump, then the pressure in the chamber was maintained at 0.01 mbar during growth. Before deposition, the transparent quartz substrate was ultrasonically degreased in trichloroethylene, acetone, and ethanol for 10 min. The target was presputtered in $Ar:O_2$ atmosphere with ratio of 60:40 for 15 min to remove contamination from the surface. The RF power during deposition was maintained at 20 W to achieve minimum surface damage during growth. All these parameters have been optimized to obtain the highest-quality ZnO thin films on transparent quartz substrate.[25,26]

### Schottky Diode Fabrication

The devices used in our study consisted of a single layer of copper phthalocyanine (CuPc) sandwiched between two electrodes of either Al and Au or Au and GZO, i.e., Al (40 nm)/CuPc (200 nm)/Au(40 nm) and GZO (300 nm)/CuPc (200 nm)/Au (40 nm). The organic layer was deposited on either Al- or GZO-coated transparent quartz substrate, then the top metal electrode of Au was evaporated on the organic layers. Each layer was deposited in a vacuum chamber at rate of 0.1 Å/s to 0.5 Å/s using an oil-free evaporation system at base pressure of $2 \times 10^{-6}$ mbar.[27,28] The thickness of the organic layer and metal electrode were measured *in situ* using a quartz crystal thickness monitor, whereas the thickness of the GZO thin film was measured using a SOPRA GES5E spectroscopic ellipsometer.

### GZO Thin-Film and Device Characterization

Resistivity ($\rho$) measurement of the GZO films was carried out using the van der Pauw method. The $\mu$ and $n$ values of the GZO films were determined by Hall measurements under a magnetic field of 1 T using a Keithley 6221 current source and Keithley 2182A nanovoltmeter. Sample thickness was measured using a SOPRA GES5E spectroscopic ellipsometer. Grazing-incidence x-ray diffraction (XRD) analysis was performed using a PANalytical X'Pert Pro system with a nickel-filtered Cu $K_\alpha$ ($\lambda$ = 1.54 Å) x-ray radiation source. X-ray photoelectron spectroscopy (XPS) data were recorded with the specimen mounted on a specially designed sample holder using an Al $K_\alpha$ laboratory x-ray source and an electron energy analyzer with five Channeltrons from Specs GmbH. The data were recorded with 20 eV pass energy and 1 eV energy resolution. Atomic force microscopy (AFM; Park XE70) was used to determine the grain size and surface morphology of the films. A Shimadzu UV-2401PC spectrophotometer was used for absorption spectroscopy in the wavelength range from 200 nm to 1000 nm. Current–voltage ($J$–$V$) and capacitance–voltage ($C$–$V$) measurements were carried out in rough vacuum ($10^{-2}$ mbar) using a Keithley picoammeter, Keithley voltage sources, and a Wayne Kerr precision component analyzer.

## RESULTS AND DISCUSSION

The XRD profiles of GZO thin films grown at 600°C with different Ga contents from 0.01% to 10% are presented in Fig. 1a. Why $T_G$ = 600°C was

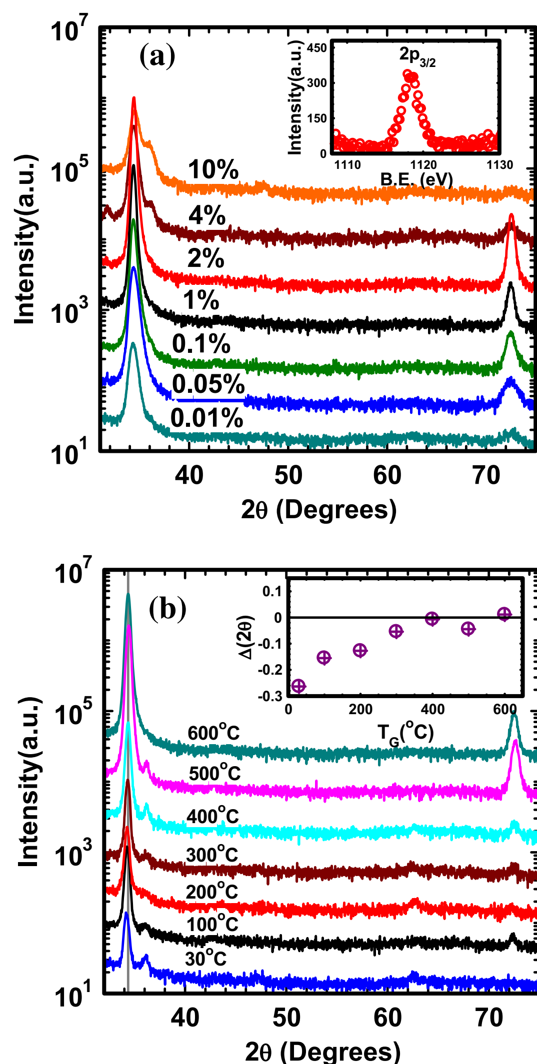


Fig. 1. (a) XRD profiles of GZO thin films prepared with different Ga contents varying from 0.01% to 10%. The $2\theta$ (002) peak around 34° shows the pronounced *c*-axis orientation of the films. The inset shows the Ga $2p_{3/2}$ core-level XPS spectrum obtained from 2% GZO thin film. (b) XRD spectra of 2% GZO films grown at different $T_G$ values. The $2\theta$ (002) peak at around 34° shows the pronounced *c*-axis orientation of the films. The inset shows the deviation of the $2\theta$ (002) signal from the ZnO powder value (shown by a horizontal line).

chosen is discussed in the next section. All the thin films showed pronounced *c*-axis orientation resulting in a strong $2\theta$ (002) peak corresponding to hexagonal wurtzite structure. The absence of any signals corresponding to $Ga_2O_3$ planes in the XRD patterns from the GZO thin films indicates homogeneous mixing of $Ga_2O_3$ with ZnO, resulting in single-phase wurtzite GZO thin films. The XRD peak observed at around 73.4° corresponds to the (004) plane of the ZnO thin film. The shift in the (002) diffraction peak of the GZO films is very small or negligible towards higher diffraction angle compared with AZO and IZO because the difference between the ionic radius of $Ga^{3+}$ (0.062 nm) and $Zn^{2+}$ (0.074 nm) is smaller than that between $Al^{3+}$ (0.053 nm) and $Zn^{2+}$ or $In^{3+}$ (0.094 nm) and $Zn^{2+}$, for which a large peak shift has been observed.[25,26] Similar behavior was observed in samples grown by PLD.[15] From Fig. 1a, it is also observed that, above a doping level of 2%, an additional peak at 36.12° corresponding to the (101) plane of the cubic phase is observed along with the (002) peak, indicating misorientation from the *c*-axis. This means that an extra phase within the ZnO thin film starts to develop along with the hexagonal wurtzite phase beyond a certain doping level due to segregation of Ga atoms either at interstitial sites ($Ga_i$) or at other nonequivalent sites instead of substitutional sites ($Ga_{Zn}$), indicating degradation of the GZO film quality with increasing Ga content. Figure 2a shows that the intensity of the (002) peak first increases with the Ga content, becoming maximum at the 2% doping level. Further doping of Ga leads to decrease in the intensity of the (002) peak due to misorientation from the *c*-axis. The inset of Fig. 1a also provides information on the oxidation state and bonding characteristics of Ga in the ZnO matrix. The binding energy of the Ga $2p_{3/2}$ peaks around 1119 eV indicates that the oxidation state[19] of Ga in the ZnO matrix is close to +3, implying donor behavior of Ga in the GZO thin films.

The XRD spectra of 2% Ga-doped ZnO obtained at different $T_G$ values are shown in Fig. 1b. The presence of the (002) peak in the XRD results implies that all films are *c*-axis oriented. The intensity of the (002) peak increases with $T_G$, becoming sharper and shifting towards higher angle from 34.07° to 34.43°, which corresponds to the $2\theta$ peak for pure ZnO powder. This can be attributed to enhanced texturing of the thin films grown at higher $T_G$ values. Similar behavior was observed for AZO films grown by RF sputtering without postgrowth annealing.[18] Figure 1b also shows the deviation of this $2\theta$ value from that for undoped ZnO powder ($2\theta \approx 34.43°$). This shift of the (002) peak can be associated with release of stress developed within the film. In addition to the (002) peak, a small peak corresponding to (101) orientation is seen at 36.2° in films grown at $T_G \leq 500°C$, disappearing in the sample grown at 600°C. This is because, as $T_G$ increases, the GZO thin films adopt a preferred *c*-axis orientation along (002) perpendicular to the quartz substrate, resulting in weakening of the (101) peak observed at 36.2°. Hence, the XRD data highlight that, at higher $T_G$, a larger amount of Ga atoms is incorporated as $Ga_{Zn}$ compared with films grown at lower $T_G$.

Figure 2b shows the full-width at half-maximum (FWHM) of the $2\theta$ (002) diffraction peak as a function of the Ga content. As the Ga content increases from 0.1% to 10%, the FWHM first decreases, reaching a lowest value of 0.38° at 2% doping, then increases at higher doping concentration. The FWHM value can be influenced by many factors such as grain size, stress distribution, and crystal

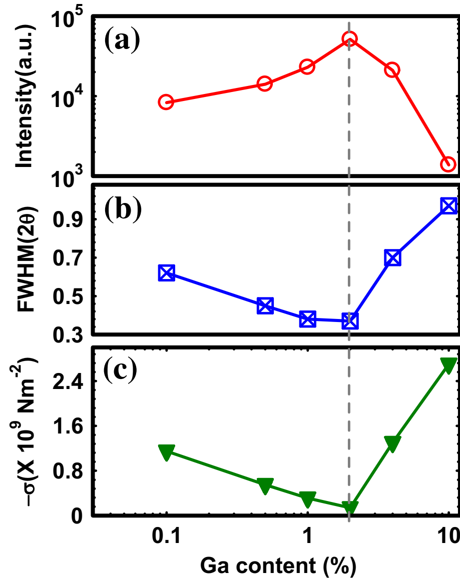


Fig. 2. Variation of the (a) intensity, (b) full-width at half-maximum (FWHM), and (c) stress induced within the GZO film as a function of Ga content from 0.1% to 10%. Connecting lines are guides to the eye.

imperfection, or misorientation from the *c*-axis.[29,30] Figure 2c shows how the stress in the GZO thin films, determined using a biaxial strain model,[31] varies with the Ga content. When Ga is incorporated into ZnO, the *c*-axis lattice constant decreases and stress release takes place, which becomes minimum at the 2% doping concentration, indicating the minimal thermal conductivity and lattice mismatch between the ZnO thin film and quartz substrate at this concentration. Therefore, precise control of the Ga doping level in ZnO is extremely important for creating a nearly stress-free environment in GZO thin films. From the FWHM, stress, and intensity of the XRD peak, we conclude that the optimal Ga content should be ≤2% to obtain high-quality, monophasic, *c*-axis-oriented GZO thin films.

Figure 3a shows the AFM topography of 2% GZO thin films grown at different $T_G$ values from 100°C to 600°C. All the films are polycrystalline in nature with grains and grain boundaries, and it is clear that the grain size increases with $T_G$. The variation of the grain size with $T_G$ is shown in the inset of Fig. 3b. Figure 3b also shows the transmission spectra of 2% GZO films grown at 100°C and 600°C. It is clear that 80% to 90% transmission in the visible to ultraviolet (UV) region was obtained in GZO thin films grown at 600°C. The 2% GZO thin films grown at 600°C were further used as transparent Schottky contacts in organic molecular semiconductor-based Schottky diodes. When the carrier concentration in *n*-type ZnO increases above a critical value of $n_C = 3.68 \times 10^{18}$ cm$^{-3}$,[18,19] known as the Mott critical concentration, the Fermi level moves up into the conduction band, resulting in metal-like behavior. This has been achieved in ZnO

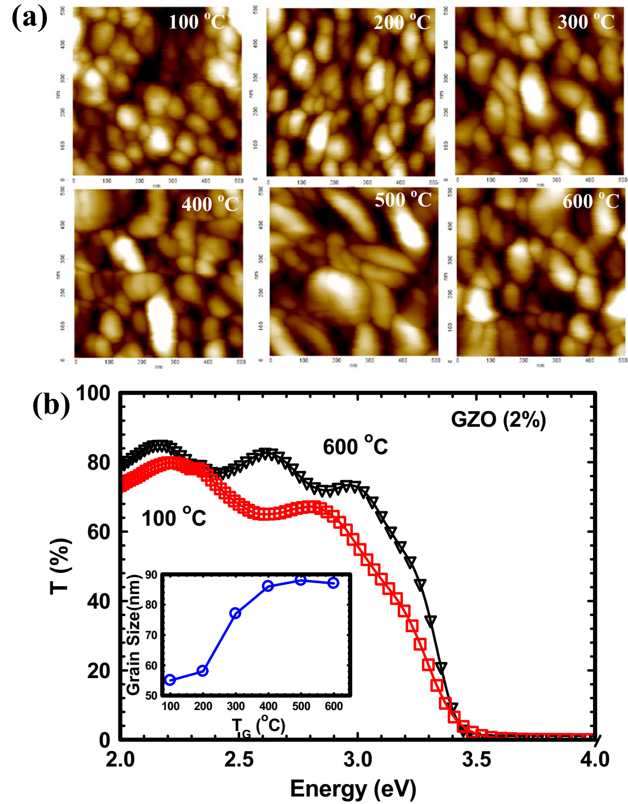


Fig. 3. (a) AFM topography (500 nm × 500 nm) of 2% GZO thin films grown at different $T_G$ values from 100°C to 600°C. (b) Transmission spectra of 2% GZO films grown at 100°C and 600°C. Inset shows the variation of grain size of 2% GZO thin films with $T_G$. Connecting lines are guides to the eye.

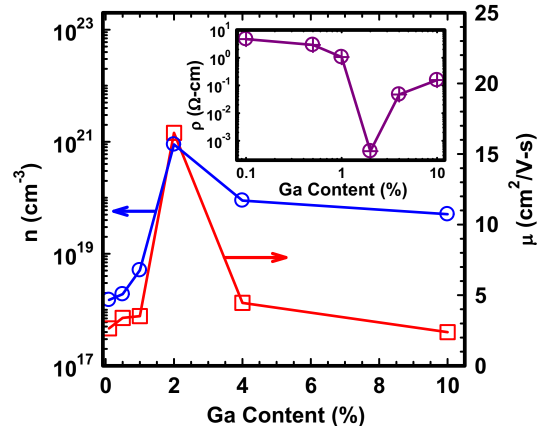


Fig. 4. Variation of carrier $n$ and $\mu$ of GZO film as a function of Ga content at 600°C. Inset shows $\rho$ of GZO film as a function of Ga content. Connecting lines are guides to the eye.

thin films doped with 2% Ga and grown at 600°C, as explained in the next section.

Figure 4 shows the electrical properties of GZO thin films with different Ga contents varying from 0.1% to 10%. As the Ga content is increased, $\mu$ and $n$

first increase and become maximum at the 2% doping level, then decrease at higher doping levels. The maximum values of $\mu$ and $n$ were found to be 16.5 $cm^2$/V-s and $8.94 \times 10^{20}$ $cm^{-3}$, respectively, resulting in a minimum $\rho$ of $4.3 \times 10^{-4}$ $\Omega$ cm in GZO thin films with 2% Ga doping concentration. The variation of $\rho$ with Ga content is also shown in the inset of Fig. 4. The initial increase of $n$ may be attributed to the efficient incorporation of Ga atoms at Zn sites. Above the 2% doping level, $n$ decreases, indicating that not all the Ga atoms in the film contribute as dopants. Excess Ga atoms at nonsubstitutional sites in ZnO films may compensate the charge carrier concentration in GZO thin films. First-principle calculations and experimental results show that Ga atoms in ZnO can occupy both substitutional ($Ga_{Zn}$) and interstitial ($Ga_i$) sites. Hence, in the case of heavily doped GZO samples, in addition to $Ga_{Zn}$, there would be $Ga_i$ and/or complexes with zinc vacancy ($V_{Zn}$), i.e., $Ga_i$–$V_{Zn}$,

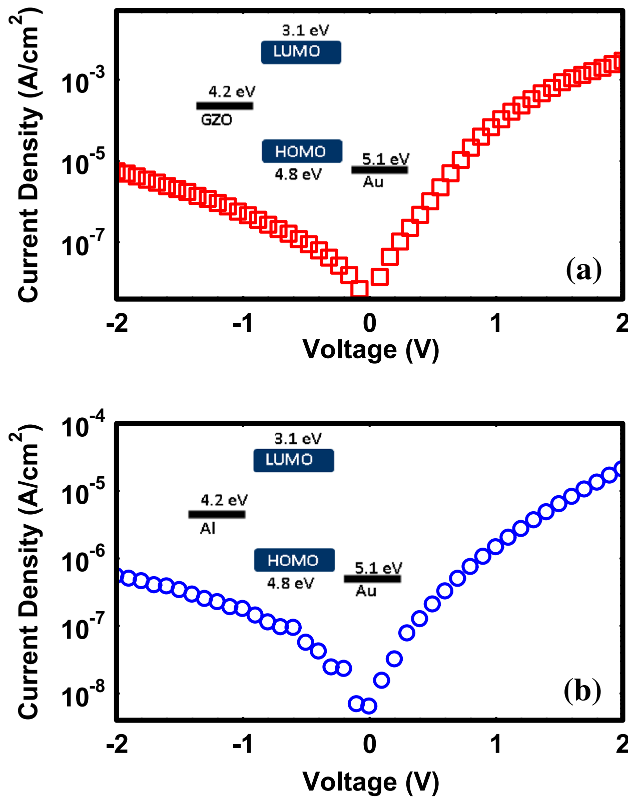


Fig. 5. $J$–$V$ characteristics of (a) GZO/CuPc/Au and (b) Al/CuPc/Au Schottky diodes. The insets show the energy band diagram of GZO/CuPc/Au and Al/CuPc/Au Schottky diodes, respectively.

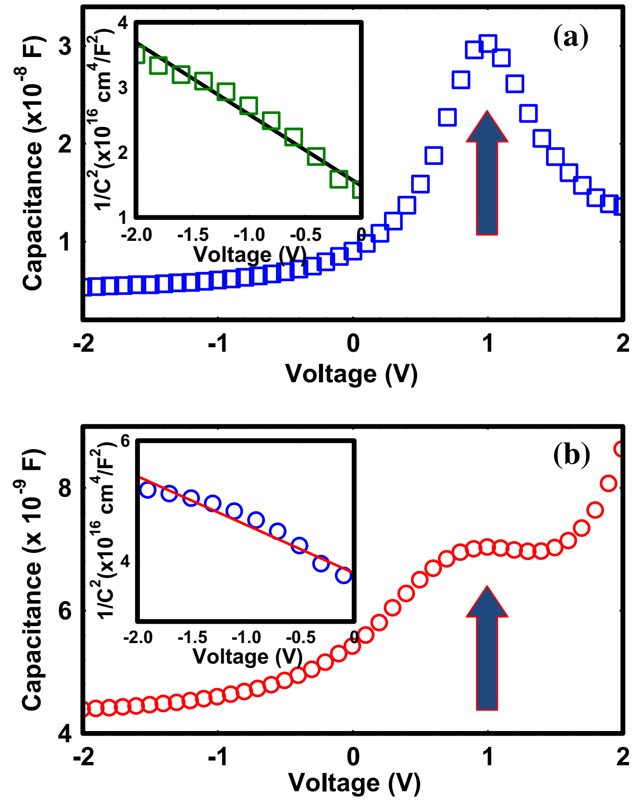


Fig. 7. Capacitance–voltage ($C$–$V$) characteristics of (a) GZO/CuPc/Au and (b) Al/CuPc/Au. Peaks indicated by arrows are the built-in potential barrier of the Schottky diodes. Insets show the voltage dependence of $1/C^2$ for the GZO/CuPc/Au and Al/CuPc/Au Schottky diodes. The straight lines are linear fits to the $1/C^2 - V$ dependence, confirming the formation of a depletion region.

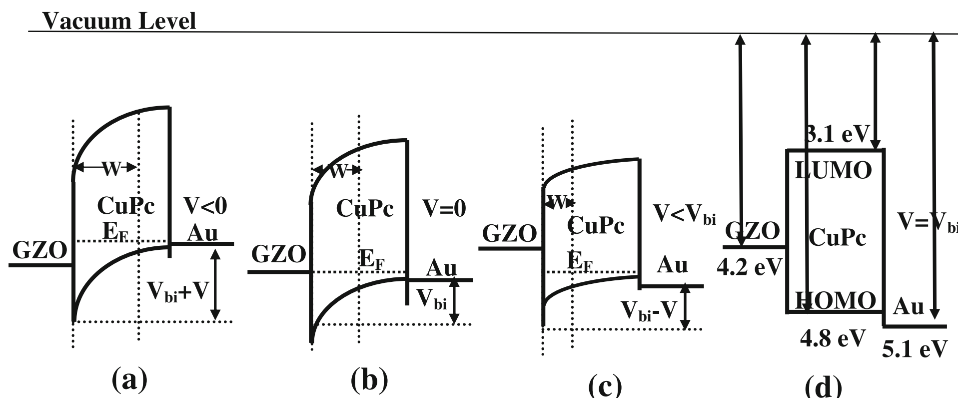


Fig. 6. Schematic energy band diagrams of GZO/CuPc/Au Schottky diode at (a) $V < 0$, (b) $V = 0$, (c) $V < V_{bi}$, and (d) $V = V_{bi}$.

which acts as an acceptor, resulting charge carrier compensation in heavily doped GZO thin films.[32–35] This is indirectly supported by the XRD data, which show misorientation of the (002) peak in the 4% and 10% doped samples. In polycrystalline thin films, grain-boundary scattering predominantly limits $\mu$. The initial increase in $\mu$ with Ga content may be due to the improvement in crystallinity as indicated by the XRD results. Above the 2% doping level, the decrease in $\mu$ can be attributed to the fact that excess Ga atoms at interstitial sites create scattering centers. Defect states at the interfaces of grain boundaries play an important role in scattering of charge carriers. Defects at grain boundary interfaces behave as electron traps and hence scatter conduction electrons. Due to the increase in $n$ with Ga doping, screening of the defect states takes place and $\mu$ increases, as has also been observed in GaN.[36–38]

Figure 5 shows a schematic energy band level diagram of the electrode work function and highest occupied molecular orbital (HOMO) and lowest unoccupied molecular orbital (LUMO) of CuPc in GZO/CuPc/Au and Al/CuPc/Au-based Schottky diodes. CuPc is a $p$-type organic molecular semiconductor with LUMO and HOMO at 3.1 eV and 4.8 eV with respect to vacuum level.[28] Al and GZO have almost the same work function (~4.2 eV), and the work function of Au is 5.1 eV.[28] There would be no barrier for holes at the Au/CuPc interface, but a barrier of 0.6 eV exists for holes at the Al/CuPc and GZO/CuPc interfaces. Hence, Al and GZO are "blocking electrodes" or Schottky contacts for holes, and as the work function of Au (~5.1 eV) is higher than the HOMO of CuPc, Au acts as a "hole-injecting electrode" or Ohmic contact for hole transport. Figure 5 shows the $J$–$V$ characteristics of the Al/CuPc/Au and GZO/CuPc/Au Schottky diodes. The current due to hole injection from positively biased Au was measured, then the current due to hole injection from Al or GZO was measured by reversing the polarity of the bias voltage. As expected, the $J$–$V$ characteristics display asymmetric behavior. The almost identical $J$–$V$ characteristics for the Al/CuPc/Au and GZO/CuPc/Au Schottky diodes establish that GZO can be used effectively as a transparent conducting electrode for organic devices. Though the rectification in the Schottky diode indicates the formation of a depletion region at the metal/semiconductor interface, the most convincing evidence for the depletion region is provided by the $C$–$V$ characteristics of the Schottky diodes. The bias dependence of the capacitance of a Schottky diode is given by[28]

$$C = \left[\frac{A^2 q \varepsilon N_A}{2(V \pm V_{bi})}\right]^{1/2}, \quad (1)$$

where $A$ = 3.14 mm$^2$ is the area of the diode, $\varepsilon$ is the permittivity of the organic layer, $N_A$ is the acceptor concentration in the organic layer, $q$ is the electronic charge, $V_{bi}$ is the built-in potential, and the positive and negative signs correspond to reverse and forward bias, respectively. The capacitance of a Schottky diode is characterized by the width of the depletion layer $W$ and is given by $C = qA/W$. According to Eq. 1, $W$ depends on the applied bias according to the relation $W \propto (V_{bi} \pm V)^{1/2}$. At $V = 0$, the Fermi level is aligned with the electrodes and a barrier for holes due to the difference in the work function of the electrodes develops at the GZO/CuPc or Al/CuPc interface. In reverse bias ($V < 0$), where we apply a positive voltage to the Schottky contact, i.e., Al or GZO, with respect to the semiconductor, the semiconductor-to-metal barrier height for holes increases by $V$, i.e., $V_{bi} + V$, whereas in the case of forward bias ($V > 0$) holes can easily flow from the Au contact to the organic semiconductor, and the barrier for holes is reduced by $V$, i.e., $V_{bi} - V$. The depletion width $W$ starts decreasing as we move from reverse to forward bias or vice versa, which can be further explained by the $C$–$V$ characteristics. Finally, the depletion width collapses at $V = V_{bi}$, resulting in the flat-band condition.[4,28] Figure 6 shows a schematic representation of the energy band diagram of the GZO/CuPc/Au diode at (a) $V < 0$, (b) $V = 0$, (c) $V < V_{bi}$, and (d) $V = V_{bi}$. Figure 7 presents the $C$–$V$ characteristics of the GZO/CuPc/Au and Al/CuPc/Au structures, showing diode-like behavior with a small peak at $V$ = 0.98 V, which is $V_{bi}$ for Al/CuPc/Au and close to the difference in work function between Au (5.2 eV) and Al (4.2 eV).[39,40] A similar peak has also been observed in GZO/CuPc/Au Schottky diodes at almost the same position, establishing that GZO behaves as a metal electrode with work function similar to Al. Hence, the electrode work functions are responsible for $V_{bi}$ in organic Schottky diodes, indicating the minimized role played by interface states at the metal/organic interface. According to Eq. 1, $1/C^2$ versus $V$ should be linear, which is also evident in Fig. 7, confirming the formation of a depletion layer in the Al/CuPc/Au and GZO/CuPc/Au Schottky diodes; the value (1.1 V) of $V_{bi}$ obtained from the $1/C^2$ versus $V$ plot is close to the value obtained from the maximum of the peak (0.98 V). The $N_A$ values obtained from the $1/C^2$ versus $V$ plots are $3.0 \times 10^{15}$/cm$^3$ and $2.0 \times 10^{15}$/cm$^3$ for the CuPc layer in Al/CuPc/Au and GZO/CuPc/Au, respectively.[28] These similar values of $N_A$ in the two devices indicate that $N_A$ is the bulk acceptor concentration and not due to interface traps.

## CONCLUSIONS

Highly conducting, transparent GZO thin films have been achieved on transparent quartz substrate by RF magnetron sputtering with varying $T_G$ and Ga content values. All thin films showed pronounced $c$-axis orientation resulting in a strong $2\theta$ (002) peak corresponding to hexagonal wurtzite structure. The minimum resistivity of $4.3 \times 10^{-4}$ Ω cm was obtained at 2% doping concentra-

tion. The transmission spectra of 2% GZO thin films obtained at $T_G$ of 600°C show almost 90% transmission in the visible to UV region. The highly conducting, transparent 2% GZO thin film was used as a Schottky contact in CuPc-based Schottky diodes.

## ACKNOWLEDGEMENTS

We acknowledge the Advanced Instrumentation Research Facility (AIRF) of JNU for providing XRD facilities for this work. This work was partly supported by DST, Govt. of India.

## REFERENCES

1. G.A. Salvatore, N. Münzenrieder, T. Kinkeldei, L. Petti, C. Zysset, I. Strebel, L. Büthe, and G. Tröster, *Nat. Commun.* 5, 2982 (2014).
2. S. Ju, A. Facchetti, Y. Xuan, J. Liu, F. Ishikawa, P. Ye, C. Zhou, T.J. Marks, and D.B. Janes, *Nat. Nanotechnol.* 2, 378 (2007).
3. P.K. Nayak, J.A. Caraveo-Frescas, Z. Wang, M.N. Hedhili, Q.X. Wang, and H.N. Alshareef, *Sci. Rep.* 4, 4672 (2014).
4. B. Singh and S. Ghosh, *Appl. Phys. Lett.* 103, 133301 (2013).
5. A. Lajn, H. von Wenckstern, M. Grundmann, G. Wagner, P. Barquinha, E. Fortunato, and R. Martins, *J. Appl. Phys.* 113, 044511 (2013).
6. P. Ray and V.R. Rao, *Appl. Phys. Lett.* 102, 064101 (2013).
7. A. Janotti and C.G. Van de Walle, *Phys. Rev. B* 76, 165202 (2007).
8. L. Schulz, L. Nuccio, M. Willis, P. Desai, P. Shakya, T. Kreouzis, V.K. Malik, C. Bernhard, F.L. Pratt, N.A. Morley, A. Suter, G.J. Nieuwenhuys, T. Prokscha, E. Morenzoni, W.P. Gillin, and A.J. Drew, *Nat. Mater.* 10, 39 (2011).
9. M. Sessolo and H.J. Bolink, *Adv. Mater.* 23, 1829 (2011).
10. R. Könenkamp, R.C. Word, and M. Godinez, *Nano Lett.* 5, 2005 (2005).
11. I. Gur, N.A. Fromer, C.-P. Chen, A.G. Kanaras, and A.P. Alivisatos, *Nano Lett.* 7, 409 (2007).
12. G.B. Murdoch, S. Hinds, E.H. Sargent, S.W. Tsang, L. Mordoukhovski, and Z.H. Lu, *Appl. Phys. Lett.* 94, 213301 (2009).
13. V. Bhosle, J.T. Prater, F. Yang, D. Burk, S.R. Forrest, and J. Narayan, *J. Appl. Phys.* 102, 023501 (2007).
14. J. Meyer, P. Görrn, S. Hamwi, H.-H. Johannes, T. Riedl, and W. Kowalsky, *Appl. Phys. Lett.* 93, 073308 (2008).
15. J.J. Berry, D.S. Ginley, and P.E. Burrows, *Appl. Phys. Lett.* 92, 193304 (2008).
16. K.-H. Lee, P.-C. Chang, T.-P. Chen, S.-P. Chang, H.-W. Shiu, L.-Y. Chang, C.-H. Chen, and S.-J. Chang, *Appl. Phys. Lett.* 102, 072104 (2013).
17. J. Steinhauser, S. Faÿ, N. Oliveira, E. Vallat-Sauvain, and C. Ballif, *Appl. Phys. Lett.* 90, 142107 (2007).
18. B. Singh, Z.A. Khan, I. Khan, and S. Ghosh, *Appl. Phys. Lett.* 97, 241903 (2010).
19. V. Bhosle, A. Tiwari, and J. Narayan, *J. Appl. Phys.* 100, 033713 (2006).
20. B. Kumar, H. Gong, and R. Akkipeddi, *J. Appl. Phys.* 98, 073703 (2005).
21. B. Singh and S. Ghosh, *J. Electron. Mater.* 43, 3217 (2014).
22. A.V. Kvit, A.B. Yankovich, V. Avrutin, H. Liu, N. Izyumskaya, U. Özgür, H. Morkoç, and P.M. Voyles, *J. Appl. Phys.* 112, 123527 (2012).
23. H.J. Ko, Y.F. Chen, S.K. Hong, H. Wenisch, T. Yao, and D.C. Look, *Appl. Phys. Lett.* 77, 3761 (2000).
24. J. Owen, M.S. Son, K.-H. Yoo, B.D. Ahn, and S.Y. Lee, *Appl. Phys. Lett.* 90, 033512 (2007).
25. Z.A. Khan and S. Ghosh, *Appl. Phys. Lett.* 99, 042504 (2011).
26. Z.A. Khan, A. Rai, S.R. Barman, and S. Ghosh, *Appl. Phys. Lett.* 102, 022105 (2013).
27. A. Sharma, S. Yadav, P. Kumar, S.R. Chaudhuri, and S. Ghosh, *Appl. Phys. Lett.* 102, 143301 (2013).
28. A. Sharma, P. Kumar, B. Singh, S.R. Chaudhuri, and S. Ghosh, *Appl. Phys. Lett.* 99, 023301 (2011).
29. K.H. Kim, K.C. Park, and D.Y. Ma, *J. Appl. Phys.* 81, 7764 (1997).
30. J.G. Lu, Z.Z. Ye, Y.J. Zeng, L.P. Zhu, L. Wang, J. Yuan, B.H. Zhao, and Q.L. Liang, *J. Appl. Phys.* 100, 073714 (2006).
31. B.C. Mohanty, Y.H. Jo, D.H. Yeon, I.J. Choi, and Y.S. Cho, *Appl. Phys. Lett.* 95, 062103 (2009).
32. D.O. Demchenko, B. Earles, H.Y. Liu, V. Avrutin, N. Izyumskaya, U. Ozgur, and H. Morkoc, *Phys. Rev. B* 84, 075201 (2011).
33. A. Zakutayev, N.H. Perry, T.O. Mason, D.S. Ginley, and S. Lany, *Appl. Phys. Lett.* 103, 232106 (2013).
34. D. Steiauf, J.L. Lyons, A. Janotti, and C.G. Van de Walle, *APL Mater.* 2, 096101 (2014).
35. D.C. Look, K.D. Leedy, L. Vines, B.G. Svensson, A. Zubiaga, F. Tuomisto, D.R. Doutt, and L.J. Brillson, *Phys. Rev. B* 84, 115202 (2011).
36. E. Baghani and S.K. O'Leary, *J. Appl. Phys.* 113, 023709 (2013).
37. N.G. Weimann, L.F. Eastman, D. Doppalapudi, H.M. Ng, and T.D. Moustakas, *J. Appl. Phys.* 83, 3656 (1998).
38. D.G. Zhao, H. Yang, J.J. Zhu, D.S. Jiang, Z.S. Liu, S.M. Zhang, Y.T. Wang, and J.W. Liang, *Appl. Phys. Lett.* 89, 112106 (2006).
39. C.H. Kim, O. Yaghmazadeh, D. Tondelier, Y.B. Jeong, Y. Bonnassieux, and G. Horowitz, *J. Appl. Phys.* 109, 083710 (2011).
40. G.G. Malliaras, J.R. Salem, P.J. Brock, and C. Scott, *Phys. Rev. B* 58, R 13411 (1998).